

# Impact of Ly $\alpha$ heating on the global 21-cm signal from the Cosmic Dawn

Raghunath Ghara<sup>1,2,3\*</sup>, Garrelt Mellema<sup>1</sup>

<sup>1</sup> *The Oskar Klein Centre, Department of Astronomy, Stockholm University, AlbaNova, SE-10691 Stockholm, Sweden*

<sup>2</sup> *Department of Natural Sciences, The Open University of Israel, 1 University Road, PO Box 808, Ra'anana 4353701, Israel*

<sup>3</sup> *Department of Physics, Technion, Haifa 32000, Israel*

Accepted XXX. Received YYY; in original form ZZZ

## ABSTRACT

The resonance scattering of Ly $\alpha$  photons with neutral hydrogen atoms in the intergalactic medium not only couples the spin temperature to the kinetic temperature but also leads to a heating of the gas. We investigate the impact of this heating on the average brightness temperature of the 21-cm signal from the Cosmic Dawn in the context of the claimed detection by the EDGES low-band experiment. We model the evolution of the global signal taking into account the Ly $\alpha$  coupling and heating and a cooling which can be stronger than the Hubble cooling. Using the claimed detection of a strong absorption signal at  $z \approx 17$  as a constraint, we find that a strong Ly $\alpha$  background is ruled out. Instead the results favour a weak Ly $\alpha$  background combined with an excess cooling mechanism which is substantially stronger than previously considered. We also show that the cooling mechanism driven by the interaction between millicharged baryons and dark matter particles no longer provides a viable explanation for the EDGES result when Ly $\alpha$  heating is taken into account.

**Key words:** radiative transfer - galaxies: formation - intergalactic medium - cosmology: theory - dark ages, reionization, first stars

## 1 INTRODUCTION

The formation of the first sources of light is one of the milestone events in the history of our Universe. These primordial sources changed the ionization and thermal state of the gas in the intergalactic medium (IGM) and thus affected the further evolution of the Universe. The period when these very first sources formed is sometimes called the ‘Cosmic Dawn’ (CD). Details regarding these early sources, such as the time of their formation, their emission properties, etc. remain unknown. Models such as in Furlanetto & Pritchard (2006); Mesinger et al. (2013); Fialkov et al. (2017); Cohen et al. (2018); Park et al. (2019); Mirocha & Furlanetto (2019), suggest that they formed around redshift 30 and their ultraviolet radiation first caused the spin temperature of the neutral hydrogen in the IGM to change due to the repetitive scattering of Lyman series photons, a process known as the Wouthuysen-Field effect (Wouthuysen 1952; Field 1958; Hirata 2006; Chuzhoy & Shapiro 2006). The same models also predict that over time X-rays produced by these sources started to heat the IGM and only much later, in what usually is called the Epoch of Reionization (EoR) sufficient numbers of ionizing photons were produced to reionize the Universe.

The 21-cm signal produced by the neutral hydrogen in the IGM during these epochs can provide us with answers to many

of the questions regarding the CD and the EoR. Therefore several efforts to detect this signal have been initiated. Two different types of experiments exist. The first type uses large interferometers to measure the spatial fluctuations of the neutral hydrogen (H I) signal in terms of statistical quantities such as the power spectrum. Examples of these are the Low Frequency Array (LOFAR)<sup>1</sup> (van Haarlem et al. 2013; Patil et al. 2017), the Giant Metrewave Radio Telescope (GMRT)<sup>2</sup> (Ghosh et al. 2012; Paciga et al. 2013), the Precision Array for Probing the Epoch of Reionization (PAPER)<sup>3</sup> (Parsons et al. 2014) and the Murchison Widefield Array (MWA)<sup>4</sup> (Bowman et al. 2013; Tingay et al. 2013). The future low-frequency component of the Square Kilometre Array (SKA-Low)<sup>5</sup> will have the sensitivity to directly probe the spatial structure of the fluctuations by producing images of the signal (Mellema et al. 2015; Ghara et al. 2017).

The second type of experiment tries to detect the sky-averaged 21-cm signal, a quantity which the interferometers are unable to measure. Such a measurement only requires a single antenna. Examples of this type are EDGES (Bowman & Rogers 2010), SARAS

\* E-mail: ghara.raghunath@gmail.com

<sup>1</sup> <http://www.lofar.org/>

<sup>2</sup> <http://www.gmrt.tifr.res.in>

<sup>3</sup> <http://eor.berkeley.edu/>

<sup>4</sup> <http://www.mwatelescope.org/>

<sup>5</sup> <http://www.skatelescope.org/>

(Patra et al. 2015), BigHorns (Sokolowski et al. 2015), SciHi (Voytek et al. 2014) and LEDA (Greenhill & Bernardi 2012).

The detection of the redshifted 21-cm signal from the EoR and CD is very challenging for all types of experiments as it is several orders of magnitude weaker than the galactic and extragalactic foreground signals at these frequencies. In addition, long integration times are needed to bring the system noise below the cosmological signal which makes calibration challenging, not only because of instrument stability but also because of the impact of time-dependent ionospheric effects. As a consequence, no undisputed detections of the signal have yet been made.

The strength of the redshifted 21-cm signal from the CD depends on the gas temperature and background Ly $\alpha$  flux which are determined by the radiation sources and the heating/cooling processes. Several heating processes such as X-ray heating (Pritchard & Furlanetto 2007; Mesinger et al. 2013; Ghara et al. 2015b, 2016; Ross et al. 2019; Islam et al. 2019), shock heating (Furlanetto & Loeb 2004) and heating due to resonance scattering of Ly $\alpha$  photons (hereafter ‘Ly $\alpha$  heating’) (Chen & Miralda-Escudé 2004; Chuzhoy & Shapiro 2007; Furlanetto & Pritchard 2006) can increase the kinetic temperature of the gas in the IGM during these epochs. However, the relative contribution of these mechanisms is uncertain. In addition to these heating processes based on known physics, unknown physics such as dark matter decay may also convey energy to the IGM (Clark et al. 2018; Mitridate & Podo 2018; Liu & Slatyer 2018a). The gas cooling is expected to be dominated by the adiabatic cooling due to the expansion of the Universe (‘Hubble cooling’) with radiative cooling due to e.g. recombinations playing a subdominant role.

Recently, Bowman et al. (2018) claimed a detection of a redshift-amplitude profile of the global 21-cm signal around redshift  $z \sim 17$  from observations with the EDGES low-band instrument. However, the measured absorption signal was found to be stronger by several factors than the signal predicted by the previous theoretical studies such as Pritchard & Furlanetto (2007); Mesinger et al. (2013); Santos et al. (2008); Ghara et al. (2015a). Explanations for the EDGES low-band results fall into two categories. The first kind assumes a lower than expected IGM temperature due to excess cooling caused by an unknown physical process such as the interaction between baryons and dark matter particles (Barkana 2018; Fialkov et al. 2018; Muñoz & Loeb 2018; Berlin et al. 2018). The second type considers the presence of an excess radio background which can also enhance the measurement of the H I signal, which is otherwise seen against the background of the Cosmic Microwave Background (CMB) (Feng & Holder 2018; Ewall-Wice et al. 2018; Fraser et al. 2018). Examples of sources which could cause such an excess radio background are supermassive black holes (Ewall-Wice et al. 2018) or supernova from first stars at  $z \gtrsim 17$  (Mirocha & Furlanetto 2019). However, models relying on such astrophysical sources are unlikely as the time scale for generating a radio background is several orders of magnitude shorter than the duration of the EDGES signal centred at redshift  $\sim 17$  (Sharma 2018). In addition the required excess background requires a  $\sim 10^3$  times stronger flux of 1-2 GHz photons than observed from local galaxies (Mirocha & Furlanetto 2019). The viable alternative is an excess radio background of cosmological origin, e.g. decay of unstable particles into dark photons with non-zero mixing angle with electromagnetism (see e.g., Pospelov et al. 2018).

Both of these explanations require the spin temperature to be strongly coupled to the gas temperature which in turn requires a strong Ly $\alpha$  background. However, these Ly $\alpha$  photons will also

heat up the gas by resonance scattering. The question is whether this heating effect has an impact on the global signal. Madau et al. (1997) estimated the heating rate due to resonance scattering assuming that the scatterings occur with atoms at rest. For this estimate, the IGM temperature would exceed the CMB temperature in a fraction of Hubble time. A subsequent paper by Chen & Miralda-Escudé (2004) included the effect of atomic thermal motions into the calculation and showed that the Ly $\alpha$  heating rate is at least three orders of magnitude lower than estimated in Madau et al. (1997). Their calculation considered heating due to photons between Ly $\alpha$  and Ly $\beta$  (so-called ‘continuum photons’) as these redshift into the Ly $\alpha$  resonance and cooling due to the cascade of higher resonance states into Ly $\alpha$  (so-called ‘injected photons’). These authors showed that these two mechanism balance at a temperature  $\sim 10$  K and thus the temperature would not increase beyond that. This low equilibrium value has prompted many works to neglect Ly $\alpha$  heating as its effect would seem to be negligible compared to for example X-ray heating. However, both these works did not consider the forbidden transition from the 2s to the 1s level of hydrogen, something which was added to the calculation by Chuzhoy & Shapiro (2007) who furthermore included the effect of deuterium. The result is a lower cooling contribution from the injected photons and which implies that the gas temperature can increase to an equilibrium value of  $\sim 100$  K prior to the reionization.

Previous studies of the global 21-cm signal in the context of the EDGES results did either not consider Ly $\alpha$  heating (see e.g., D’Amico et al. 2018; Liu & Slatyer 2018b; Schneider 2018; Barkana et al. 2018; Nebrin et al. 2019) or used the erroneously low values from Chen & Miralda-Escudé (2004) (see e.g., Fialkov & Barkana 2019; Venumadhav et al. 2018). In this study, we for the first time adopt the calculation of the Ly $\alpha$  heating rates from Chuzhoy & Shapiro (2007) and investigate its impact on the global 21-cm signal from the CD. We include excess cooling so as to be able to reproduce EDGES low-band observations. We will consider models which use an excess radio background in a future work. We explore the parameter space of Ly $\alpha$  heating and excess cooling to study the absorption profile of the global signal to find combinations of parameters that agree with the EDGES low-band results.

We have organised the paper in the following way. In Section 2 we describe the analytical model we use to calculate the evolution of the global 21-cm signal, including the heating rates due to resonance scattering of the Ly $\alpha$  photons. We first present results for a phenomenological excess cooling rate in Section 3, followed by an investigation of a physically motivated excess cooling rate in Section 4. We conclude in Section 5. Throughout the paper we use the following set of cosmological parameters  $\Omega_m = 0.32$ ,  $\Omega_B = 0.049$ ,  $\Omega_\Lambda = 0.68$ ,  $h = 0.67$ ,  $\sigma_8 = 0.83$  and  $n_s = 0.96$  (Planck Collaboration et al. 2016).

## 2 MODEL FOR 21-CM SIGNAL

### 2.1 Analytical model

The 21-cm signal from the H I gas is measured as the differential brightness temperature against the CMB and can be written as

$$\delta T_b = 27 x_{\text{HI}} (1 + \delta_B) \left( \frac{\Omega_B h^2}{0.023} \right) \sqrt{\frac{0.15}{\Omega_m h^2} \frac{1+z}{10}} \left( 1 - \frac{T_\gamma}{T_S} \right) \text{ mK}, \quad (1)$$

where  $x_{\text{HI}}$ ,  $\delta_B$ ,  $T_S$  and  $T_\gamma = 2.73 \times (1+z)$  K denote the neutral fraction, density contrast, spin temperature of the hydrogen gas and CMB temperature at redshift  $z$ , respectively.

We adopt an analytic approach to model the expected 21-cm signal in the presence of spin temperature fluctuations. This approach follows previous works such as [Pritchard & Furlanetto \(2007\)](#); [McQuinn et al. \(2005\)](#). It incorporates Ly $\alpha$ , UV and X-ray photons from the sources which are taken to be associated with dark matter halos. The number of dark matter halos at a given redshift is determined using the Press-Schechter halo mass function. We assume that only halos with virial temperatures above  $10^4$  K contribute. The model estimates the volume averaged ionization fractions of the highly ionized H II regions ( $x_i$ ) and of the mostly neutral gas in the IGM outside these H II regions ( $x_e$ ). We assume the temperature of the ionized H II regions to be  $\sim 10^4$  K. The gas temperature ( $T_K$ ) of the largely neutral medium outside the H II regions is calculated using the various heating and cooling processes.

The heating rate due to resonance scattering as well as the spin temperature coupling depend critically on the number of Ly $\alpha$  photons emitted from the sources. To estimate the average Ly $\alpha$  photon flux, we follow the method from [Furlanetto & Pritchard \(2006\)](#). We assume a power law spectrum  $\epsilon_s(\nu) = f_\alpha A_\alpha \nu^{-\alpha_s-1}$  between Ly $\alpha$  and Ly $\beta$  and between Ly $\beta$  and the Lyman limit, where the power law indices  $\alpha_s$  can differ. The spectral index  $\alpha_s$  between Ly $\alpha$  and Ly $\beta$  is taken to be 0.14 which corresponds to population II type sources. The normalization factor  $A_\alpha$  is estimated such that the number of Ly $\alpha$  photons per baryon in the range Ly $\alpha$ -Ly $\beta$  is 6520 for  $f_\alpha = 1$ . The spectral index in the range Ly $\alpha$ -Lyman limit is adjusted so that the total number of photons per baryon for this wavelength regime is 9690. The parameter  $f_\alpha$  determines the production rate of the Ly $\alpha$  photons from the stars. The heating rate due to Ly $\alpha$  scattering is described below in Section 2.2.

To model the X-ray heating, we follow [Pritchard & Furlanetto \(2007\)](#) and assume that the emissivity of X-ray photons from the sources follows the star formation rate density. We use an X-ray spectral distribution given by

$$\epsilon_X(\nu) = \frac{L_0}{h\nu_0} \left( \frac{\nu}{\nu_0} \right)^{-\alpha_X-1}, \quad (2)$$

with  $L_0 = f_X \times 10^{41} \text{ erg s}^{-1} \text{ Mpc}^{-3}$ ,  $h\nu_0 = 1 \text{ keV}$ . For our fiducial X-ray source we choose the X-ray efficiency parameter to be  $f_X = 1$  and the spectral index of the X-ray spectrum to be  $\alpha_X = 0.5$ . Note that for most of our results we will set  $f_X = 0$  as we want to focus on the effect of Ly $\alpha$  heating. This makes our results conservative as additional X-ray heating will only further increase the gas temperature.

Finally our model also includes the effect of ionizing UV radiation. The rate of emission of the UV photons per baryon is

$$\Lambda_i = \zeta \frac{df_{\text{coll}}}{dt}. \quad (3)$$

The ionization efficiency parameter  $\zeta = N_{\text{ion}} \times f_{\text{esc}} \times f_\star$  depends on the average number of ionizing photons per baryon produced in the stars ( $N_{\text{ion}}$ ), the star formation efficiency ( $f_\star$ ) and the escape fraction of the UV photons ( $f_{\text{esc}}$ ). All these quantities are uncertain during the CD and EoR. In this study, we assume  $N_{\text{ion}} = 4000$  which corresponds to population II types of stars,  $f_\star = 0.1$  and  $f_{\text{esc}} = 0.1$  for modelling reionization. We note however that for most of our results ionization levels remain very low and do not impact the global 21-cm signal.

## 2.2 Heating due to resonance scattering

To estimate the heating rates due to the resonance scattering, we follow the calculations of [Chuzhoy & Shapiro \(2007\)](#). Photons

emitted with frequencies between Ly $\alpha$  and Ly $\beta$  frequency ('continuum photons') will redshift to the Ly $\alpha$  frequency at which point they suffer resonance scattering by H I. This process will heat up the gas. On the other hand, photons with a wavelength between Ly $\beta$  and Lyman limit will be absorbed by the hydrogen atoms after redshifting to Ly $\beta$  or other higher Lyman series lines. If higher resonance or excited states first decay to  $2p$  state and then to the ground state, one Ly $\alpha$  photon will be emitted. In contrast to the continuum photons, the emission of the Ly $\alpha$  photons ('injected photons') due to the cascade of from the higher levels will cool the gas. The spectrum gets affected once the photons redshift through the Ly $\alpha$  resonance. The intensity  $J(\nu)$  at a frequency  $\nu$  in the vicinity of the resonance frequency  $\nu_\alpha$  can be written as ([Chuzhoy & Shapiro 2007](#)),

$$J(x) = J(0)e^{-\frac{2\pi\gamma x^3}{3a} - 2\eta x}, \quad (4)$$

for the injected photons. The above expression also hold for the continuum photons with  $x > 0$ , otherwise

$$J(x) = 2\pi J_0 \gamma a^{-1} \int_{-\infty}^x e^{\frac{2\pi\gamma(z^3-x^3)}{3a} + 2\eta(z-x)} dz. \quad (5)$$

where

$$\begin{aligned} x &= (\nu/\nu_\alpha - 1)/(2k_B T_K/mc^2)^{1/2}, \\ a &= A_{21}(2k_B T_K/mc^2)^{-1/2}/4\pi\nu_\alpha, \\ \gamma &= \tau_{\text{GP}}^{-1}(1 + 0.4/T_S)^{-1}, \\ \eta &= [h\nu_\alpha/(2k_B T_K mc^2)^{1/2}][(1 + 0.4/T_S)/(1 + 0.4/T_K)]. \end{aligned} \quad (6)$$

Here  $k_B$ ,  $m$ ,  $c$  and  $A_{21}$  are the Boltzmann constant, mass of hydrogen atom, speed of light and the Einstein spontaneous emission coefficient of Ly $\alpha$  transition respectively. The quantities  $\tau_{\text{GP}}$  and  $J_0$  are the Gunn-Peterson optical depth and the UV intensity at a frequency far away from  $\nu_\alpha$ , respectively.

The quantity  $J(0)$  can be expressed as,

$$\frac{J(0)}{J_0} = \frac{\pi\zeta (J_{1/3}(\zeta) - J_{-1/3}(\zeta))}{\sqrt{3}} + {}_1F_2(1; 1/3, 2/3, -\zeta^2/4) \quad (7)$$

where  $\zeta = \sqrt{16\eta^3 a/9\pi\gamma}$ ,  ${}_1F_2$  is hyper-geometric function,  $J_{1/3}$  and  $J_{-1/3}$  are the Bessel functions of first kind respectively.

The total heating/cooling rate due to the resonance scattering can be written as,

$$\left. \frac{d \log T_K}{d \log t} \right|_{\text{heating}} = \frac{2t}{3k_B T_K} H_\alpha, \quad (8)$$

where  $t$  represents time,  $H_\alpha$  is the rate of exchange of total energy by the photons due to resonance scattering.

$$H_\alpha = \dot{N}_\alpha \left( \Delta E_c + \frac{J_i}{J_c} \Delta E_i \right) \quad (9)$$

where  $\dot{N}_\alpha$  denotes the number of photons per hydrogen atom that pass through resonance scattering per unit time. The ratio of injected and continuum photons  $J_i/J_c$  depends on the source's surface temperature. We choose  $J_i/J_c \approx 0.1$  which corresponds to a source with an effective temperature  $\lesssim 5 \times 10^4$  K which corresponds approximately to population II type of sources ([Chuzhoy & Shapiro 2007](#)). The quantities  $\Delta E_c$  and  $\Delta E_i$  are the total energy gain by the gas due to a resonance scattering by the continuum and injected photons respectively. This can be written as,

$$\Delta E(x) = \frac{(h\nu)^2}{mc^2} \int \frac{J(x)}{J_0} \phi(x) dx \quad (10)$$

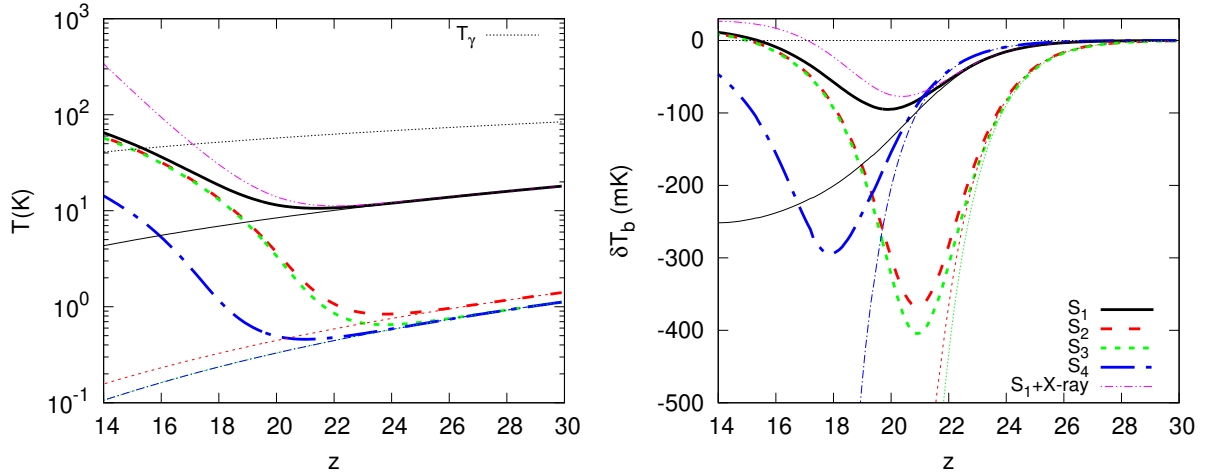


**Figure 1.** Left-hand panel: The redshift evolution of the gas temperature for the different scenarios described in Section 3.1, also see Table 1. The thin lines show the cases without Ly $\alpha$  heating, the thick lines the cases with Ly $\alpha$  heating. The double dot-dashed curve shows the case of model S<sub>1</sub> with X-ray heating but without Ly $\alpha$  heating. The black dotted curve indicates the evolution of the CMB temperature with redshift. Right-hand panel: The redshift evolution of the volume averaged differential brightness temperature  $\delta T_b$  for the same scenarios.

where  $\phi(x)$  is the normalized scattering cross-section. Note that Chuzhoy & Shapiro (2007) also considered the heating contribution from deuterium in their studies. Here we have not included this and thus our calculations somewhat underestimate the actual heating rates.

### 2.3 Cooling processes

The gas temperature of the IGM is one of the key quantities which determines the strength and nature of the 21-cm signal from the CD. As the heating and cooling processes during those epochs are uncertain, the gas temperature as well as the signal are poorly understood. The analytical method used in this study incorporates the adiabatic cooling due to the expansion of the Universe which dominates over radiative processes such as the collisional-ionization cooling, recombination cooling, collisional excitation cooling, free-free cooling, etc. After Compton scattering with CMB photons ceases to be important, this Hubble cooling causes the average gas temperature to evolve as  $T_K \propto (1+z)^2$ . For standard physics, the post-recombination gas temperature is easily calculated, as can for example be done with the publicly available code RECFAST (Seager et al. 1999). The results show that for our cosmological parameters the  $T_K \propto (1+z)^2$  relation is valid below  $z_0 \approx 138$ . Expressed in the same form as the Ly $\alpha$  heating rate in Equation 8, this adiabatic or Hubble cooling is given as

$$\left. \frac{d \log T_K}{d \log t} \right|_H = -\frac{4}{3}.$$

However, as pointed out by Bowman et al. (2018) this cooling process is unable to explain the strong absorption signal at redshift 17 found in the EDGES low-band results as it requires a lower temperature than can be achieved using standard cosmological models. In order to reproduce the EDGES results we therefore need to include an excess cooling rate in our calculations. Here we make two choices. In Section 3 we use a simple phenomenological excess cooling model and in Section 4 we use a physically motivated excess cooling rate based on interactions between dark matter particles and baryons.

Scenarios	$f_\alpha$	$\alpha$	$\beta$	$\delta T_{b,\min}$	$z(\delta T_{b,\min})$	$\Delta z$
S <sub>1</sub>	1.0	0.0	0.0	-95.1	19.9	4.6
S <sub>2</sub>	1.0	-1.0	0.0	-367.1	20.9	3.7
S <sub>3</sub>	1.0	-1.0	-0.1	-404.6	20.9	3.6
S <sub>4</sub>	0.1	-1.0	-0.1	-294.4	17.9	4.2

**Table 1.** The Ly $\alpha$  efficiency and excess cooling parameters for the four different scenarios considered in Section 3.1. Also shown are the quantities which describe the resulting absorption profile,  $\delta T_{b,\min}$ ,  $z(\delta T_{b,\min})$  and  $\Delta z$  which represent the minimum brightness temperature, its corresponding redshift and the FWHM of the absorption profiles, respectively.

### 3 PHENOMENOLOGICAL COOLING MODEL

In this section, we consider a simple phenomenological cooling rate inspired by Mirocha & Furlanetto (2019), given by

$$\left. \frac{d \log T_K}{d \log t} \right|_{\text{cool}} = \alpha \left[ \frac{1+z}{1+z_0} \right]^\beta. \quad (11)$$

The parameters  $\alpha \leq 0$  and  $\beta$  determine the strength and redshift dependence of the excess cooling rate respectively. We only apply this excess cooling rate for redshifts  $z \leq z_0$ . However, in principle,  $z_0$  could be treated as a free parameter.

To gain insight into the impact of Ly $\alpha$  heating on the volume averaged 21-cm signal from the CD, we first show the results for a number individual scenarios (Section 3.1). After this we will explore the parameter space made up of  $\alpha$ ,  $\beta$  and the average Ly $\alpha$  flux (Section 3.2). Lastly, we will investigate scenarios that can explain the strong absorption signal as reported by the EDGES low-band observation (Section 3.3).



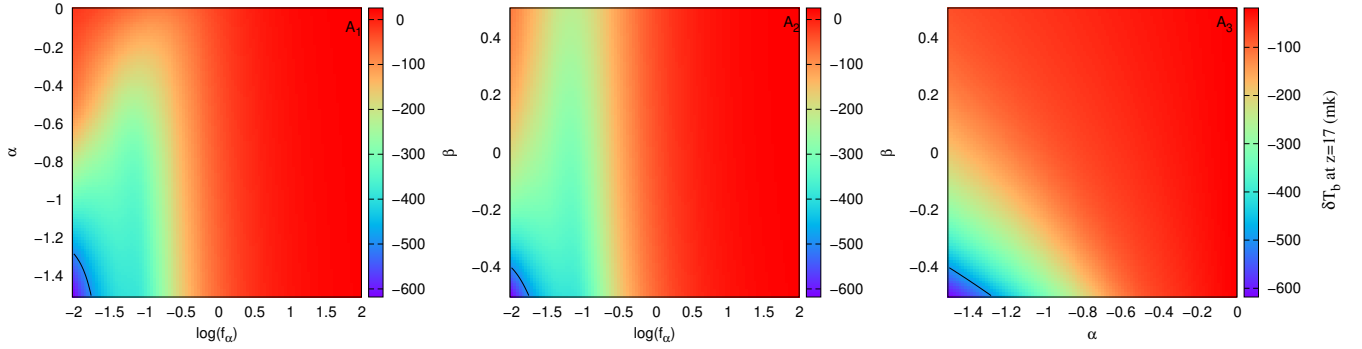


**Figure 2.** The different panels show the averaged brightness temperature at redshift 17. We vary two parameters at a time in these slices, the third parameter is fixed such that each slice contains the lowest brightness temperature at redshift 17 for the entire parameter space. The third parameter values are  $\beta = -0.5$ ,  $\alpha = -1.5$  and  $f_\alpha = 0.01$  for panels  $A_1$ ,  $A_2$  and  $A_3$ , respectively. The black contours represent -500 mK brightness temperature as reported by the EDGES low-band observation.

Parameters	Min range	Max Range
$f_\alpha$	0.01	100.0
$\alpha$	-1.5	0.0
$\beta$	-0.5	0.5

**Table 2.** The range of the three parameters for the phenomenological cooling model explored in this study.

### 3.1 Exploratory scenarios

We choose four different sets of parameters to study the impact of different parameters/processes on the evolution of  $\delta T_b$ . The parameters for these scenarios are listed in Table 1. The fiducial model  $S_1$  has  $\alpha = 0$  and therefore does not include any excess cooling. The left-hand panel of Fig. 1 presents the redshift evolution of the average gas temperature of the neutral regions in the IGM for these four choices. For each, we consider two cases, namely without (thin lines) and with (thick lines) Ly $\alpha$  heating. For the choice of no excess cooling  $S_1$  we also consider a case without Ly $\alpha$  heating but with heating by X-ray sources (thin double dot-dashed curve).

For the cases without Ly $\alpha$  and X-ray heating, the temperature keeps decreasing over time as no other heating mechanisms are included in these scenarios. When we include Ly $\alpha$  heating, it impacts the gas temperatures as early as redshift 22 in all these scenarios. For the scenario without excess cooling, the gas temperature increases to  $\sim 60$  K at redshift  $\sim 14$  which is roughly consistent with the results of Chuzhoy & Shapiro (2007). The small difference is due to ignoring the contribution from deuterium in our calculations. When we instead of Ly $\alpha$  heating include X-ray heating according to the description in Section 2.1, the gas temperature for  $S_1$  increases more rapidly and reaches  $\sim 300$  K by  $z \sim 14$ . This is why Ly $\alpha$  heating is often ignored in simulations as X-ray heating will quickly dominate. However, if X-ray heating is inefficient or absent, Ly $\alpha$  heating will have a non-negligible impact on the IGM temperature.

As scenarios  $S_2$ – $S_4$  include excess cooling, the Cosmic Dawn starts at lower gas temperatures than for  $S_1$ . In  $S_2$  the excess cooling does not have a redshift dependence, in  $S_3$  it increases with

time.  $S_4$  has the same excess cooling parameters as  $S_3$  but a ten times lower Ly $\alpha$  efficiency. When including the heating due to the scattering of Ly $\alpha$  photons, it impacts the temperatures in  $S_2$  and  $S_3$  earlier compared to  $S_1$ , although the background Ly $\alpha$  flux densities for these models are identical. This is due to the fact that the Ly $\alpha$  heating rates increases as the kinetic temperature decreases (see Equation 8). As expected the heating starts later for a lower Ly $\alpha$  background ( $S_4$ ).

Scenarios  $S_1$ ,  $S_2$  and  $S_3$  each start with different temperatures. However, by  $z \sim 16$  they all reach almost the same equilibrium temperature due to Ly $\alpha$  heating. For  $\alpha = 1$  the excess cooling can thus not compete with Ly $\alpha$  heating. For the case of a lower Ly $\alpha$  flux ( $S_4$ ), the heating is delayed and remains weaker compared to the other scenarios.

The right-hand panel of Fig. 1 shows the redshift evolution of the global 21-cm signal corresponding to the nine scenarios ( $S_1$  through  $S_4$  with and without Ly $\alpha$  heating and  $S_1$  with X-ray heating). Note that we always include the Ly $\alpha$  coupling for the spin temperature, even in those models where we ignore Ly $\alpha$  heating. As for all these scenarios the IGM remains highly neutral at redshifts  $> 14$ , the average brightness temperature is mostly determined by the gas temperature and the strength of the Ly $\alpha$  coupling. As the background Ly $\alpha$  flux is low at high redshift ( $z \sim 30$ ), the coupling between  $T_S$  and  $T_K$  is weak and  $T_S$  remains close to  $T_\gamma$ . This makes  $\delta T_b \approx 0$  at those redshifts. As more sources form with time, Ly $\alpha$  coupling becomes stronger and the signal starts to appear in absorption, i.e., with a negative sign. However, different heating processes can increase the gas temperature and eventually  $\delta T_b$  transitions from absorption to emission. This produces a characteristic trough-like feature in the redshift evolution of  $\delta T_b$ , which we refer to as the ‘absorption profile’.

In the absence of Ly $\alpha$  or X-ray heating,  $\delta T_b$  decreases with redshift as  $T_K$  decreases with time and the signal remains in absorption until reionization ends. In such cases,  $\delta T_b$  slowly decreases to  $\sim -250$  mK at redshift  $\sim 15$  for  $S_1$  without excess cooling (thin solid line), while  $\delta T_b$  rapidly decreases to values below  $\sim -500$  mK at redshift  $\lesssim 20$  for models  $S_2$  through  $S_4$  which include excess cooling (thin long-dashed, short-dashed and dot-dashed lines).

In the presence of Ly $\alpha$  heating, the increase of gas temperature as early as redshift  $\sim 20$  resists the decrease of  $\delta T_b$  with time and produces prominent absorption profiles (thick lines). The

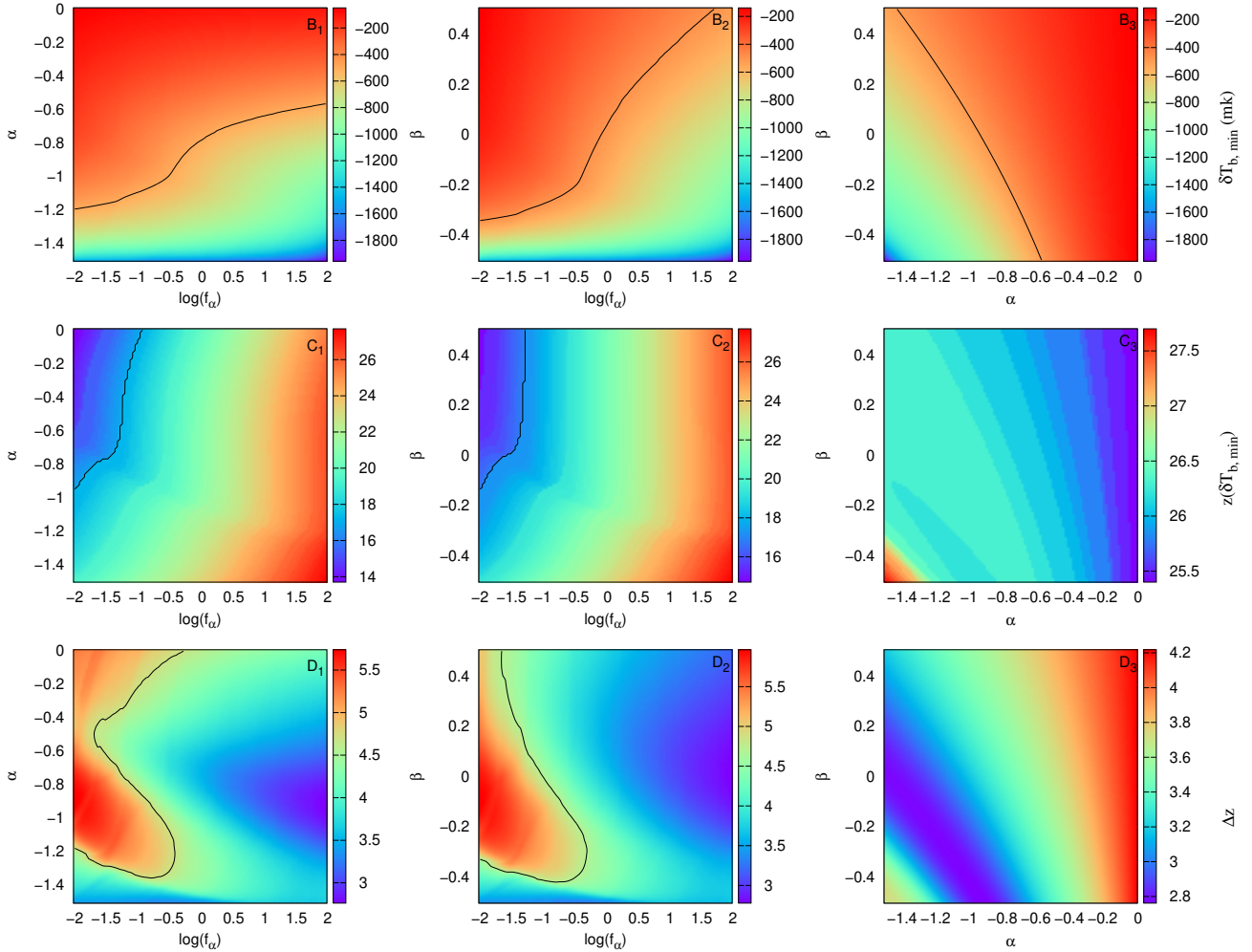


**Figure 3.** The upper panels represent the minimum brightness temperature throughout Cosmic Dawn  $\delta T_{b,\min}$  in 2D slices through the parameter space. The third parameter is fixed such that the slices contain the lowest brightness temperature obtained while exploring the entire 3D parameter space. In this case, the third parameter values are  $\beta = -0.5$ ,  $\alpha = -1.5$  and  $f_\alpha = 100$  which correspond to panels  $B_1$ ,  $B_2$  and  $B_3$  respectively. The middle row panels represent the associated redshifts,  $z(\delta T_{b,\min})$  and the bottom panels the FWHM  $\Delta z$  of the absorption profile of these models. The contours from top to bottom panels of the figure represent  $\delta T_{b,\min} = -500$  mK,  $z(\delta T_{b,\min}) = 17.2$  and  $\Delta z = 4.7$  respectively which characterize the absorption profile as reported by the EDGES low-band observation.

minimum  $\delta T_b$  values of these profiles are much less deep than the corresponding signals from the no heating cases, demonstrating the large impact Ly $\alpha$  heating has. For example in scenario  $S_1$  the absorption profile does not reach below -100 mK and for  $S_2$  and  $S_3$  not below -400 mK.

The absorption profiles can be described by the minimum value of the brightness temperature ( $\delta T_{b,\min}$ ), the corresponding redshift  $z(\delta T_{b,\min})$  and the full width at half maximum (FWHM) of the absorption profile ( $\Delta z$ ). We list the values for the cases with Ly $\alpha$  heating in Table 1. These numbers clearly depend on the excess cooling rate and Ly $\alpha$  heating rates. We see the absorption profiles are much stronger and appear earlier for models  $S_2$  and  $S_3$  than for model  $S_1$ . This is due to the excess cooling in the former models which results in a lower initial gas temperature compared to  $S_1$ . The values for the  $\Delta z$  are lower when excess cooling is present.

When the Ly $\alpha$  background is lower ( $f_\alpha = 0.1$ , scenario  $S_4$ ) the absorption profile becomes less deep, widens and appears later

compared to the scenario which has  $f_\alpha = 1$  ( $S_3$ ), even though the gas temperature is actually lower. However, the profile can still reach a minimum of  $\sim -300$  mK, below what can be achieved without excess cooling.

For completeness, the right-hand panel of Fig. 1 also shows the differential brightness temperature evolution for the scenario without excess cooling and Ly $\alpha$  heating but with X-ray heating (thin dot-dot-dashed curve). Due to the higher temperatures, this absorption profile is less deep and somewhat narrower than the corresponding case with Ly $\alpha$  heating (thick solid curve).

### 3.2 Parameter space study

Now we will explore the parameter space of excess cooling ( $\alpha$  and  $\beta$ ) and Ly $\alpha$  flux ( $f_\alpha$ ) to find the impact on the absorption signal from the CD in terms of absorption profile parameters  $\delta T_{b,\min}$ ,  $z(\delta T_{b,\min})$  and  $\Delta z$ . The details of the parameter space are given

in Table 2. As the excess cooling is due to unknown processes, the parameter ranges for  $\alpha$  and  $\beta$  chosen here are somewhat arbitrary. However, as we will see this range covers the most interesting results in terms of the absorption feature and the EDGES low-band results.

We will study the global 21-cm signal around redshift  $\sim 17$  which corresponds to  $z(\delta T_{b,\min})$  of the EDGES low-band detection. The different panels of Fig. 2 represent the value of the differential brightness temperature at redshift 17 in 2D slices through the 3D parameter space. For these slices, the third parameter is chosen such that these slices contain the lowest brightness temperature at  $z = 17$  within the explored parameter space. The values are  $\beta = -0.5$  (panel A<sub>1</sub>),  $\alpha = -1.5$  (panel A<sub>2</sub>) and  $f_\alpha = 0.01$  (panel A<sub>3</sub>).

The resonance photons impact the signal in two ways: (i) heating due to resonance scattering decreases for a lower background Ly $\alpha$  flux, (ii) coupling of  $T_S$  with  $T_K$  decreases for a lower Ly $\alpha$  background. These two effects create the vertical feature in  $\delta T_b$  around  $f_\alpha \sim 0.1$  in panels A<sub>1</sub> and A<sub>2</sub>. In the presence of significant Ly $\alpha$  heating (e.g. for  $f_\alpha > 1$ ), the amplitude of  $\delta T_b$  at redshift 17 remains small for all values of  $\alpha$  and  $\beta$ . As shown in panel A<sub>3</sub>, strong excess cooling ( $\alpha \sim -1.5$  and  $\beta \sim -0.5$ ) can produce a deep absorption feature but only for a very weak Ly $\alpha$  flux, reaching values as low as  $-600$  mK for  $f_\alpha \sim 0.01$ .

We note that the color bar associated with the panels of Fig. 2 represents  $\delta T_b$  at redshift 17, not  $\delta T_{b,\min}$  for the choice of parameters. This figure shows that  $\delta T_b \sim -500$  mK at redshift 17 is only possible for a weak Ly $\alpha$  background and strong excess cooling rates as shown by the contours in the panels. However, this does not mean that the values of  $\delta T_b$  in this figure are equal to  $\delta T_{b,\min}$ , the minimum of the absorption profiles. Thus, we can not directly compare these with the EDGES low-band observations. However, we can see that a large part of the parameter space corresponds to  $\delta T_b$  values larger than  $-500$  mK and thus, should be excluded by the EDGES observation. We will present a detailed investigation of this in Section 3.3.

First we will investigate the behaviour of absorption profiles over the parameter space. The top row of panels of Fig. 3 show 2D slices of  $\delta T_{b,\min}$  through the entire parameter space. As in Fig. 2, the third parameter is chosen such that these slices contain the lowest value of  $\delta T_{b,\min}$  obtained within the entire parameter space. In this case, the values for the third parameter are  $\beta = -0.5$ ,  $\alpha = -1.5$  and  $f_\alpha = 100$  which correspond to the left, middle and right panels, respectively. The middle row of panels shows the associated redshift  $z(\delta T_{b,\min})$  of the minimum of the absorption profiles and the bottom row the corresponding FWHM  $\Delta z$ .

Panels B<sub>1</sub> and B<sub>2</sub> show that  $\delta T_{b,\min}$  decreases with increasing  $f_\alpha$  as the coupling between  $T_S$  and  $T_K$  becomes stronger. However, this also implies that Ly $\alpha$  heating becomes efficient earlier and thus the minima of the absorption profiles appear at higher redshifts when increasing  $f_\alpha$  (see panels C<sub>1</sub>, C<sub>2</sub>). As shown in panel B<sub>3</sub>,  $\delta T_{b,\min}$  decreases for lower values of  $\alpha$  and  $\beta$  which corresponds to stronger excess cooling and also in this case  $z(\delta T_{b,\min})$  shifts towards higher redshifts (panel C<sub>3</sub>). The CD starts with a lower gas temperature for smaller values of  $\alpha$  and  $\beta$ . As the Ly $\alpha$  heating rate increases for lower temperatures, Ly $\alpha$  heating become efficient earlier for a stronger excess cooling model. These results are consistent with our findings in Section 3.1.

The bottom row of Fig. 3 shows the corresponding FWHM  $\Delta z$ . The dependence of  $\Delta z$  on the parameters is more complex compared to what we saw for  $\delta T_{b,\min}$  and  $z(\delta T_{b,\min})$ . Here we have to keep in mind a few aspects. One is that all models reach

their equilibrium temperature due to Ly $\alpha$  heating approximately at the same redshift for a fixed Ly $\alpha$  background (as we have seen in Section 3.1). Secondly, the initial temperature (at  $z = 30$ ) of these models decreases rapidly with stronger cooling parameters. The absorption profile becomes deeper and shifts towards higher redshift for a larger excess cooling rate. On the other hand, the Ly $\alpha$  heating starts earlier and  $\delta T_b$  of these profiles approaches zero at a similar redshift. These two facts make  $\Delta z$  decrease initially with the increase of excess cooling rate for a fixed  $f_\alpha$  as shown in panel D<sub>3</sub>. However,  $\Delta z$  starts increasing for  $\alpha < -1$  and  $\beta < 0$  as the initial temperature of these models becomes smaller and the minimum of the absorption profiles shifts towards higher redshifts. On the other hand, Ly $\alpha$  heating becomes efficient earlier for a larger value of  $f_\alpha$  which decrease  $\Delta z$  for a fixed excess cooling (see panels D<sub>1</sub> and D<sub>2</sub>).

The black lines in Fig. 3 correspond to the absorption profile parameters estimated from the EDGES low-band observation. However, as these slices correspond to the minimum  $\delta T_b$  calculated by exploring the whole 3D parameter space, an interpretation of EDGES results from these contours is difficult. We therefore now turn our attention to the parts of the parameter space that are consistent with the EDGES absorption profile.

### 3.3 Interpretation of EDGES low-band results

Bowman et al. (2018) reported a measurement of a 21-cm absorption profile with  $\delta T_{b,\min} = -500^{+200}_{-500}$  mK with  $z(\delta T_{b,\min})$  and  $\Delta z$  equivalent to  $78 \pm 1$  MHz and  $19^{+4}_{-2}$  MHz, respectively. We will investigate what part of our parameter space agrees with this observation. However, we do not consider the detailed shape of the absorption profile as reported in Bowman et al. (2018), nor use parameter estimation techniques such as Markov chain Monte Carlo. Instead, we consider the values of  $\delta T_{b,\min}$ ,  $z(\delta T_{b,\min})$  and  $\Delta z$  corresponding to the profile to compare with the absorption profiles produced by our model. We would like to remind the reader that we have not included any X-ray heating in this parameter space study.

Fig. 4 presents which values for our parameters agree with the EDGES low band results. The left-hand panel shows a 2D plot for parameters  $\alpha$  and  $\beta$  where the colour of each point represents the average value of  $f_\alpha$  for which the values of  $\alpha, \beta$  are consistent with the EDGES observation. We see that two specific ranges of cooling parameters produce the desired profile, the broader of the two bands for a weak Ly $\alpha$  background flux ( $f_\alpha < 0.08$ ) and the narrower one for a very weak Ly $\alpha$  background ( $f_\alpha < 0.01$ ). The broader band is characterized by a strong but not too strong cooling around the redshift of the absorption profile ( $-2 \lesssim (d \log T_K / d \log t)_{\text{cool}} \lesssim -1.2$ ) and the narrower band by a stronger value of  $(d \log T_K / d \log t)_{\text{cool}} \sim -2.5$ . This can also be characterized through the temperature which the IGM would achieve in the absence of Ly $\alpha$  heating. For the cooling parameters in the broader of the two bands, this temperature is between 0.2 and 0.3 K and between 0.05 and 0.06 K for the narrower band. For stronger cooling than shown in the left-hand panel,  $\delta T_{b,\min}$  will be lower and will shift towards higher redshifts. Similarly,  $z(\delta T_{b,\min})$  will shift towards higher redshifts for larger values of  $f_\alpha$ .

The right-hand panel of Fig. 4 shows a 3D representation of our parameter space where the colour indicates the  $\chi^2$  value. We define  $\chi^2$  error in this plot as

$$\chi^2 = \sum_{i=1,3} \left( \frac{M_i - O_i}{\sigma_i} \right)^2, \quad (12)$$

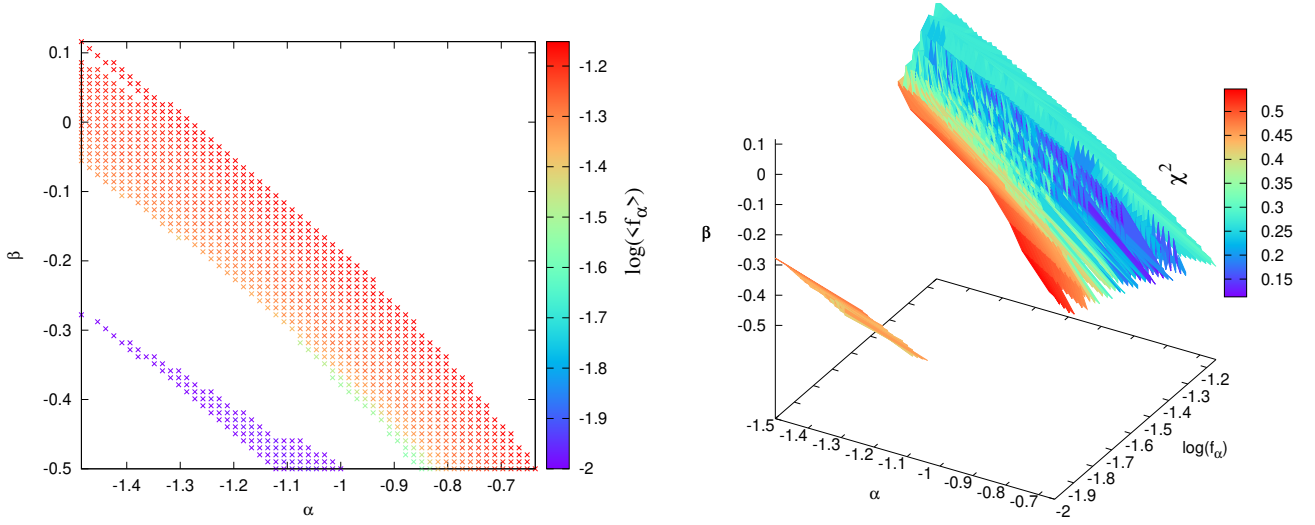


**Figure 4.** Left-panel: The crosses indicate the values of the excess cooling parameters  $\alpha$  and  $\beta$  which produce absorption profiles that agree with the EDGES low band results within a  $1\sigma$  error. The colour bar represents the average values of  $f_\alpha$  for these models. Right panel: 3D plot of the parameter space which agrees with the EDGES low band results. The colour bar shows the  $\chi^2$  error as defined in Equation 12.

where  $i$  represents there parameters to define the absorption profile used in this study,  $M$  and  $O$  are the model and observation parameters respectively and  $\sigma_i$  represents the  $1\sigma$  error on the measured parameters considered here. One can notice that for a certain choice of cooling parameters a range of  $f_\alpha$  values can satisfy the agreement condition. However, all  $f_\alpha$  values are low. The isolated region  $f_\alpha = 0.01$  corresponds to deeper absorption profiles with  $\delta T_{b,\min} \lesssim -500$  mK while the other region has absorption depths  $\delta T_{b,\min} \sim -300$  mK.

One thing to keep in mind that we have ignored all other heating processes such as X-ray heating, etc. If any other additional energy is added to the IGM, the excess cooling would have to compensate for this in order for the absorption profile to remain consistent with the EDGES result. In other words, the cooling rates derived here should be considered as lower limits. For example, the combination  $f_\alpha \lesssim 0.1$ ,  $\alpha \sim -1.5$  and  $\beta \sim 0.1$  corresponds to the minimum excess cooling required to achieve the strong signal reported by EDGES. This minimum excess cooling rate is similar to the Hubble cooling rate at redshift 17.

#### 4 PHYSICALLY MOTIVATED COOLING MODEL

So far we have considered a simple phenomenological form for the cooling rate as given by Equation 11. Now we will consider a physically motivated cooling model based on the interaction between cold dark matter and baryonic particles. Such interactions have the potential to cool the baryonic gas efficiently and explain the EDGES results (Barkana 2018; Muñoz & Loeb 2018; Barkana et al. 2018; Fialkov et al. 2018). However, most of these interaction scenarios are highly constrained by limits from stellar cooling and fifth force experiments. This rules out scenarios in which the cooling of the gas occurs through Rutherford-like scattering with a dominant component of the dark matter. However, a scenario in which cooling is caused by interactions of electrons and protons with a small ( $\sim 1\%$ ) fraction of millicharged dark matter particles

is currently not entirely ruled out (see e.g., Muñoz & Loeb 2018) although only in a very small part of parameter space (Barkana et al. 2018).

The cooling rate for this scenario can be written as

$$\left. \frac{d \log T_K}{d \log t} \right|_{\text{cool,DMB}} = \frac{4\dot{Q}_b}{9 H T_K}, \quad (13)$$

where the cooling rate of the baryon  $\dot{Q}_b$  can be expressed as the sum of the contributions due to collisions with electrons or protons as targets  $t$  (Muñoz & Loeb 2018),

$$\dot{Q}_b = \frac{n_\chi x_e}{1 + f_{\text{He}}} \sum_{t=e,p} \frac{m_t m_\chi}{(m_t + m_\chi)^2} \frac{\bar{\sigma}_t}{u_{\text{th},t}} \times \left[ \sqrt{\frac{2}{\pi}} \frac{e^{-r_t^2/2}}{u_{\text{th},t}^2} (T_\chi - T_K) + m_\chi \frac{F(r_t)}{r_t} \right]. \quad (14)$$

Here,  $x_e$  is the residual electron fraction after recombination and  $f_{\text{He}} \approx 0.08$  is the primordial helium fraction. The symbol  $m$  stands for mass, where  $e$ ,  $p$  and  $\chi$  stand for electron, proton and dark matter, respectively. The number density of millicharged dark matter is  $n_\chi = f_{\text{dm}} \times \rho_d / m_\chi$  where  $\rho_d$  is the dark matter mass density and  $f_{\text{dm}}$  is the fraction of millicharged dark matter.  $T_K$  and  $T_\chi$  represent the temperatures of the baryon gas and the dark matter respectively. The function  $F(r_t)$  is defined as

$$F(r_t) = \text{Erf}\left(\frac{r_t}{\sqrt{2}}\right) - \sqrt{\frac{2}{\pi}} r_t e^{-r_t^2/2}, \quad (15)$$

where  $r_t = v_{\chi b} / u_{\text{th},t}$ , with  $v_{\chi b}$  the relative velocity between the baryons and the dark matter and  $u_{\text{th},t}^2 = T_K / m_t + T_\chi / m_\chi$  the (iso)thermal sound speed of the DM- $t$  fluid. Finally, the rate also depends on the interaction cross-section between the millicharged dark matter particles and a target  $t$ ,  $\bar{\sigma}_t$ . We define a charge parameter  $\epsilon = e_\chi / e$  where  $e_\chi$  and  $e$  are the dark matter and electron charge respectively. The interaction cross-section is assumed to scale with relative velocity as  $\bar{\sigma}_t = \frac{2\pi\alpha_f^2\epsilon^2\xi}{\mu_{\chi t}^2 v_{\chi b}^4}$  where  $\alpha_f$  is the fine-structure



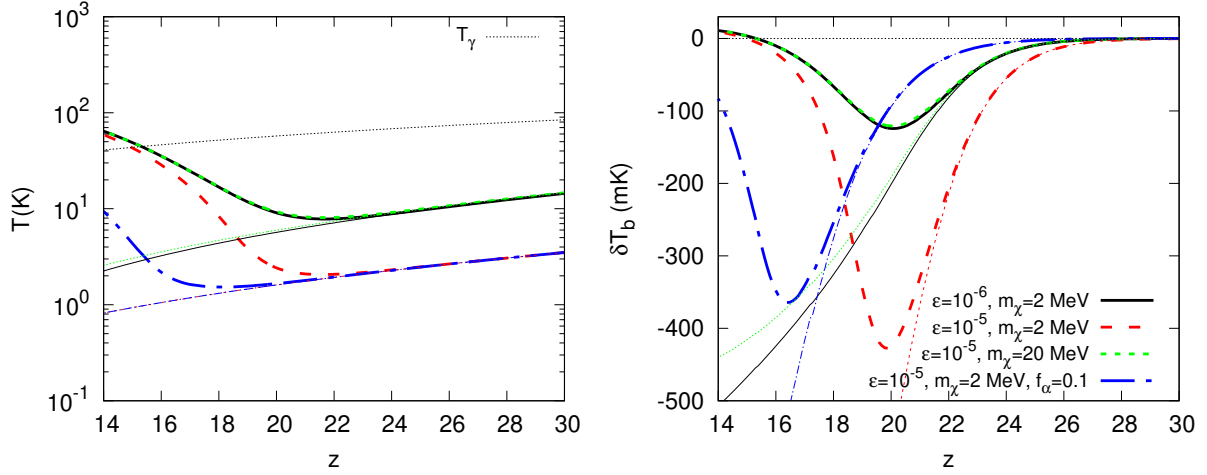


**Figure 5.** Left-hand panel: The redshift evolution of the gas temperature for the different models where cooling of the gas is dominated by interaction with millicharged dark matter. The thin lines show the cases without Ly $\alpha$  heating and the thick lines the cases with Ly $\alpha$  heating. Different curves correspond to different combinations of  $m_\chi$  and  $\epsilon$ . All curves have been calculated for  $f_\alpha = 1$  except the thick and thin dot-dashed blue curves which use  $f_\alpha = 0.1$ . The fraction of millicharged dark matter is set to  $f_{\text{dm}} = 0.01$ . The black dotted curve in the left panel indicates the evolution of the CMB temperature with redshift. Right-hand panel: The redshift evolution of the volume averaged differential brightness temperature  $\delta T_b$  for the same scenarios.

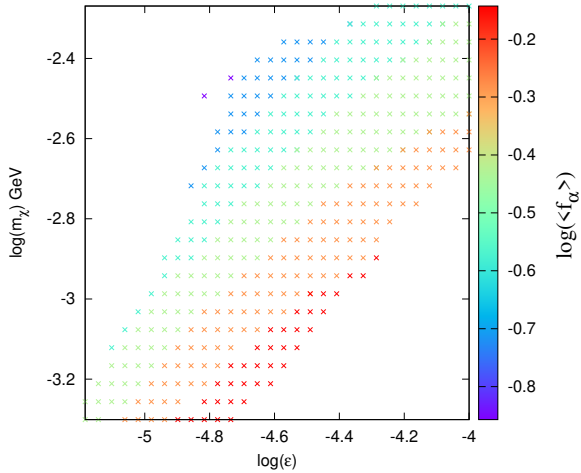


**Figure 6.** Parameter study for the millicharged dark matter cooling model. The parameters  $\epsilon$  and  $m_\chi$  represent the charge and the mass of the dark matter particles. The markers indicate the values of the parameters which produce absorption profiles that agree with the EDGES low band results within a  $1\sigma$  error. The colour bar represents the average values of  $f_\alpha$  for these models.

constant,  $\xi$  is the Debye logarithm and  $\mu_{\chi t}^2$  is the reduced mass of the dark matter and target. We refer to Muñoz & Loeb (2018) for more details on the various terms in Equation 14.

We follow the approach as in Muñoz & Loeb (2018) and solve the set of differential equations to track the evolution of the temperatures of the gas and dark matter. We initialize  $T_K = T_\gamma$  and  $T_\chi = 0$  at  $z = 1010$ . We assume that the initial distribution of  $v_{\chi b,0}$  is Gaussian with a root-mean-square value of  $29 \text{ km s}^{-1}$ . We solve the set of equations for many values  $v_{\chi b,0}$  taken from this distribution and in the end estimate the velocity averaged gas temperatures and brightness temperature.

We will vary two parameters for the cooling rate as described in Equation 13, namely  $\epsilon$ , the charge of the dark matter particles and their mass  $m_\chi$ . We keep the fraction of millicharged dark matter fixed at  $f_{\text{dm}} = 0.01$  throughout this study. Figure 5 shows the redshift evolution of the gas temperature (left panel) and the brightness temperature (right panel) for three different combinations of  $m_\chi$  and  $\epsilon$ . The thin lines show the results with Ly $\alpha$  coupling but *without* Ly $\alpha$  heating and the thick lines include Ly $\alpha$  heating. We use  $f_\alpha = 1$ , except for the dot-dashed line which has  $f_\alpha = 0.1$ . These results illustrate the trends associated with the different parameters.

It should first of all be noted that these results are very similar to those shown in Fig. 1. In absence of Ly $\alpha$  heating, a cooling rate with the combination of  $m_\chi \sim 2 \text{ MeV}$  and  $\epsilon \sim 10^{-6}$  cools the gas to a temperature  $\sim 4 \text{ K}$  at redshift 17 which is sufficient to produce a signal which agrees with the EDGES low-band observations, consistent with the results of Barkana et al. (2018); Muñoz & Loeb (2018). However, as expected, the Ly $\alpha$  heating prevents the gas temperature to reach such a low value, even for  $f_\alpha = 1$ . The cooling, as well as the signal, becomes stronger for larger values of  $\epsilon$  as this raises the interaction cross-section. On the other hand, increasing  $m_\chi$  lowers the cooling rate and the signal. As above, we find that the absorption profile shifts towards lower redshifts for lower values of  $f_\alpha$ . These trends suggest that this cooling model might satisfy the EDGES results for the following two cases: (i) a higher cooling rate than estimated by Barkana et al. (2018); Muñoz & Loeb (2018) which can arise due to either a larger  $\epsilon$  or a smaller  $m_\chi$ , (ii) a lower Ly $\alpha$  flux to keep the heating low at  $z \sim 17$ .

Next, we vary the parameter  $\epsilon$  from  $10^{-7}$  to  $10^{-4}$  and  $m_\chi$  from  $0.5 \text{ MeV}$  to  $1 \text{ GeV}$  while we keep the range of  $f_\alpha$  the same as used previously. Equivalent to Fig. 4 for the phenomenological model, Fig. 6 presents the parts of parameter space which agree with the EDGES measurements. Note that similar to the earlier case, we have not considered any heating mechanism other than heating due to scattering of the Ly $\alpha$  photons. As expected, we find the required Ly $\alpha$  flux in this scenario has to be less than 1 as shown by the color bar. Note however that the  $f_\alpha$  values found are higher

than what we obtained for the phenomenological cooling model. This suggests that the millicharged dark matter cooling process produces a larger cooling rate at redshift  $\sim 17$  than the explored range in the previous cooling model.

While [Barkana et al. \(2018\)](#); [Muñoz & Loeb \(2018\)](#) conclude that  $\epsilon \gtrsim 10^{-6}$  will be required for  $m_\chi = 2$  MeV to reach agreement with the EDGES results, Fig. 6 suggests a larger value of  $\epsilon \gtrsim 1.5 \times 10^{-5}$  for the same dark matter mass. The required Ly $\alpha$  flux for these  $m_\chi$  and  $\epsilon$  values corresponds to  $f_\alpha \sim 0.3$ . Clearly, a larger dark matter-baryon interaction cross-section is required when Ly $\alpha$  heating is taken into account.

However, the possible parameter space of the millicharge model in Fig. 6 that can explain the EDGES result is disfavoured by the constraints from stellar and super-nova cooling, big bang nucleosynthesis and a range of particle physics experiments. Specifically, as shown in fig. 4 in [Barkana et al. \(2018\)](#), these constraints require  $m_\chi \gtrsim 10$  MeV and for these values we do not find any solutions that are consistent with the EDGES results. We therefore conclude that the millicharged dark matter model no longer offers a viable explanation for the absorption signal claimed by the EDGES team.

## 5 DISCUSSIONS & CONCLUSIONS

In this study we have considered the impact of the heating from resonance scattering of Ly $\alpha$  photons in the IGM during the Cosmic Dawn on models with excess cooling constructed to explain the deep absorption feature around  $z \sim 17$  reported by the EDGES team. This heating is an inevitable result of the resonance scattering which is needed to couple the spin temperature to the gas temperature, the only known process which can produce an observable 21-cm signal from the IGM at these redshifts. The required excess cooling requires new physics and thus its cause remains uncertain. We explored two possibilities, one simple phenomenological form of cooling and one physically motivated one relying on the interaction of putative millicharged dark matter particles with protons and electrons.

For these two scenarios we investigate the evolution of the average differential brightness temperature of the 21-cm signal. We explore a three-dimensional parameter space defined by two parameters describing the excess cooling ( $\alpha$  and  $\beta$  for the phenomenological model;  $\epsilon$  and  $m_\chi$  for the millicharged dark matter) and one parameter setting the strength of the Ly $\alpha$  background ( $f_\alpha$ ) to study the global 21-cm signal from the CD. The main findings of the paper are listed below.

Without any excess cooling, Ly $\alpha$  heating can start heating the IGM as early as redshift 22 for a typical emissivity of  $\sim 10000$  photons per baryon between Ly $\alpha$  and the Lyman limit. Although this heating rate is smaller than the usually assumed X-ray heating rates, it can still increase the gas temperature to several tens of K which is the equilibrium temperature between the heating by the continuum photons and cooling by the injected photons. This is consistent with previous studies such as [Chuzhoy & Shapiro \(2007\)](#). For this case, we find an absorption signal of depth  $\sim -100$  mK at redshift  $\sim 20$ .

When including excess cooling, the Cosmic Dawn starts with a very cold IGM. In such cases, Ly $\alpha$  heating becomes efficient earlier and rapidly increases the IGM temperature to the equilibrium temperature. For these cases, we find absorption signals which can be factors 3 – 4 deeper than without excess cooling.

The exploration of the parameter space of the excess cooling

rate parameters and the Ly $\alpha$  background shows that the EDGES low-band results can only be reproduced for strong excess cooling combined with a weak Ly $\alpha$  background. This puts an upper bound on the background Ly $\alpha$  flux which is  $\sim 15$  times lower than our fiducial choice for the phenomenological cooling model, while for the millicharged dark matter model this upper limit is only a factor  $\sim 2$  below the fiducial value. Thus the sources at redshift  $\sim 17$  emit fewer Ly $\alpha$  photons or the star formation efficiency is lower than expected. This result disagrees with the findings of [Mirocha & Furlanetto \(2019\)](#) who claim that the star formation efficiency should be higher than expected in order to produce the strong Ly $\alpha$  background needed to achieve strong coupling between the spin and gas temperatures. However, these authors did not consider the effect of Ly $\alpha$  heating.

Although we find that the millicharged dark matter model can reproduce the EDGES results for a relatively low Ly $\alpha$  background and some combinations of DM charge and mass, these combinations are actually ruled out by constraints from stellar and super-nova cooling, big bang nucleosynthesis and a range of particle physics experiments ([Barkana et al. 2018](#)). Including Ly $\alpha$  heating therefore removes this model as a feasible explanation for the EDGES results.

In our exploration of the parameter space for the phenomenological model we frequently found interesting models at the edge of the parameter ranges that we considered. We did not explore a larger range of values as the trend is quite clear: only fairly strong cooling which without Ly $\alpha$  heating would give gas temperatures below  $\sim 0.3$  K around  $z \approx 17$  combined with a weak Ly $\alpha$  background ( $f_\alpha \lesssim 0.06$ ) can reproduce the EDGES low-band results. Possibly even stronger cooling with an even weaker Ly $\alpha$  background would also give consistent results but such models become increasingly unlikely.

In general, Ly $\alpha$  heating works against all kind of excess cooling models that might explain the EDGES result and will potentially provide strong bounds on their parameters. The same is true for the alternative solutions which rely on a stronger radiation background at the Rayleigh-Jeans tail of the CMB (see e.g., [Pospelov et al. 2018](#)). However, we leave the study of the impact of Ly $\alpha$  heating on those types of models to a future study.

We did not explore the impact of changing the source population. In our models, all halos with a virial temperature above  $10^4$  K contribute to the Ly $\alpha$  background. Obviously increasing this limit would also reduce the background and possibly lead to models in which fiducial values for  $f_\alpha$  combined with strong excess cooling could reproduce the EDGES low-band absorption profile. Lowering the minimum virial mass would only increase the Ly $\alpha$  background and thus require even lower values for  $f_\alpha$ . We also did not explore the impact of the star formation efficiency parameter  $f_*$  and the SED. However, for the redshift regime which we explore these parameters are degenerate with  $f_\alpha$ .

We thus find that heating due to resonance scattering with Lyman series photons may have a significant impact during the Cosmic Dawn and thus should be taken into account when modelling the 21-cm signal. Although we do find that for a fiducial value of X-ray heating ( $f_X = 1$ ), the Ly $\alpha$  heating is subdominant, many authors explore a wide range of values for  $f_X$  including low values for which Ly $\alpha$  heating will dominate over X-ray heating (e.g. [Cohen et al. 2017](#); [Greig & Mesinger 2018](#); [Monsalve et al. 2019](#)). We note that none of these papers actually include the effect of Ly $\alpha$  heating.

Models to explain the absorption feature seen in the EDGES results rely on Ly $\alpha$  coupling to produce an observable signal and

thus any excess cooling needs to overcome the heating caused by this coupling. As shown in this paper, this pushes for example the millicharged dark matter model into a regime ruled out by other constraints. It remains to be seen if there exist any physically motivated excess cooling processes which can explain the EDGES results.

## ACKNOWLEDGEMENTS

The authors would like to thank Hannah Ross, Paul Shapiro, Anastasia Fialkov, Sambit Giri, Benedetta Ciardi, Avery Meiksin, Piero Madau, Tirthankar Roy Choudhury for useful discussions regarding this work. We also like to thank an anonymous referee whose comments have encouraged us to explore the millicharged dark matter model. We have used resources provided by the Swedish National Infrastructure for Computing (SNIC) (proposal number SNIC 2018/3-40) at PDC, Royal Institute of Technology, Stockholm.

## REFERENCES

- Barkana R., 2018, *Nature*, **555**, 71
- Barkana R., Outmezguine N. J., Redigol D., Volansky T., 2018, *Phys. Rev. D*, **98**, 103005
- Berlin A., Hooper D., Krnjaic G., McDermott S. D., 2018, *Phys. Rev. Lett.*, **121**, 011102
- Bowman J. D., Rogers A. E. E., 2010, *Nature*, **468**, 796
- Bowman J. D., et al., 2013, *Publ. Astron. Soc. Australia*, **30**, e031
- Bowman J. D., Rogers A. E. E., Monsalve R. A., Mozdzen T. J., Mahesh N., 2018, *Nature*, **555**, 67
- Chen X., Miralda-Escudé J., 2004, *ApJ*, **602**, 1
- Chuzhoy L., Shapiro P. R., 2006, *ApJ*, **651**, 1
- Chuzhoy L., Shapiro P. R., 2007, *ApJ*, **655**, 843
- Clark S. J., Dutta B., Gao Y., Ma Y.-Z., Strigari L. E., 2018, *Phys. Rev. D*, **98**, 043006
- Cohen A., Fialkov A., Barkana R., Lotem M., 2017, *MNRAS*, **472**, 1915
- Cohen A., Fialkov A., Barkana R., 2018, *MNRAS*, **478**, 2193
- D’Amico G., Panci P., Strumia A., 2018, *Phys. Rev. Lett.*, **121**, 011103
- Ewall-Wice A., Chang T.-C., Lazio J., Doré O., Seiffert M., Monsalve R. A., 2018, *ApJ*, **868**, 63
- Feng C., Holder G., 2018, *ApJ*, **858**, L17
- Fialkov A., Barkana R., 2019, *MNRAS*, **486**, 1763
- Fialkov A., Cohen A., Barkana R., Silk J., 2017, *MNRAS*, **464**, 3498
- Fialkov A., Barkana R., Cohen A., 2018, *Phys. Rev. Lett.*, **121**, 011101
- Field G. B., 1958, *Proceedings of the IRE*, **46**, 240
- Fraser S., et al., 2018, *Physics Letters B*, **785**, 159
- Furlanetto S. R., Loeb A., 2004, *ApJ*, **611**, 642
- Furlanetto S. R., Pritchard J. R., 2006, *MNRAS*, **372**, 1093
- Ghara R., Choudhury T. R., Datta K. K., 2015a, *MNRAS*, **447**, 1806
- Ghara R., Datta K. K., Choudhury T. R., 2015b, *MNRAS*, **453**, 3143
- Ghara R., Choudhury T. R., Datta K. K., 2016, *MNRAS*, **460**, 827
- Ghara R., Choudhury T. R., Datta K. K., Choudhuri S., 2017, *MNRAS*, **464**, 2234
- Ghosh A., Prasad J., Bharadwaj S., Ali S. S., Chengalur J. N., 2012, *MNRAS*, **426**, 3295
- Greenhill L. J., Bernardi G., 2012, preprint, ([arXiv:1201.1700](https://arxiv.org/abs/1201.1700))
- Greig B., Mesinger A., 2018, *MNRAS*, **477**, 3217
- Hirata C. M., 2006, *MNRAS*, **367**, 259
- Islam N., Ghara R., Paul B., Choudhury T. R., Nath B. B., 2019, *MNRAS*, **487**, 2785
- Liu H., Slatyer T. R., 2018a, arXiv e-prints, [p. arXiv:1803.09739](https://arxiv.org/abs/1803.09739)
- Liu H., Slatyer T. R., 2018b, *Phys. Rev. D*, **98**, 023501
- Madau P., Meiksin A., Rees M. J., 1997, *ApJ*, **475**, 429

- McQuinn M., Furlanetto S. R., Hernquist L., Zahn O., Zaldarriaga M., 2005, *ApJ*, **630**, 643
- Mellema G., Koopmans L., Shukla H., Datta K. K., Mesinger A., Majumdar S., 2015, *Advancing Astrophysics with the Square Kilometre Array (AASKA14)*, **p. 10**
- Mesinger A., Ferrara A., Spiegel D. S., 2013, *MNRAS*, **431**, 621
- Mirocha J., Furlanetto S. R., 2019, *MNRAS*, **483**, 1980
- Mitridate A., Podo A., 2018, *Journal of Cosmology and Astro-Particle Physics*, **2018**, 069
- Monsalve R. A., Fialkov A., Bowman J. D., Rogers A. E. E., Mozdzen T. J., Cohen A., Barkana R., Mahesh N., 2019, *ApJ*, **875**, 67
- Muñoz J. B., Loeb A., 2018, arXiv e-prints, [p. arXiv:1802.10094](https://arxiv.org/abs/1802.10094)
- Nebrin O., Ghara R., Mellema G., 2019, *J. Cosmology Astropart. Phys.*, **2019**, 051
- Paciga G., et al., 2013, *MNRAS*, **433**, 639
- Park J., Mesinger A., Greig B., Gillet N., 2019, *MNRAS*, **484**, 933
- Parsons A. R., et al., 2014, *ApJ*, **788**, 106
- Patil A. H., et al., 2017, *ApJ*, **838**, 65
- Patra N., Subrahmanyam R., Sethi S., Udaya Shankar N., Raghunathan A., 2015, *ApJ*, **801**, 138
- Planck Collaboration et al., 2016, *A&A*, **594**, A13
- Pospelov M., Pradler J., Ruderman J. T., Urbano A., 2018, *Phys. Rev. Lett.*, **121**, 031103
- Pritchard J. R., Furlanetto S. R., 2007, *MNRAS*, **376**, 1680
- Ross H. E., Dixon K. L., Ghara R., Iliev I. T., Mellema G., 2019, *MNRAS*, **487**, 1101
- Santos M. G., Amblard A., Pritchard J., Trac H., Cen R., Cooray A., 2008, *ApJ*, **689**, 1
- Schneider A., 2018, *Phys. Rev. D*, **98**, 063021
- Seager S., Sasselov D. D., Scott D., 1999, *ApJ*, **523**, L1
- Sharma P., 2018, *MNRAS*, **481**, L6
- Sokolowski M., et al., 2015, *Publ. Astron. Soc. Australia*, **32**, e004
- Tingay S. J., et al., 2013, *Publications of the Astronomical Society of Australia (PASA)*, **30**, 7
- Venumadhav T., Dai L., Kaurov A., Zaldarriaga M., 2018, *Phys. Rev. D*, **98**, 103513
- Voytek T. C., Natarajan A., Jáuregui García J. M., Peterson J. B., López-Cruz O., 2014, *ApJ*, **782**, L9
- Wouthuysen S. A., 1952, *AJ*, **57**, 31
- van Haarlem M. P., et al., 2013, *A&A*, **556**, A2

This paper has been typeset from a  $\text{\LaTeX}$  file prepared by the author.